

MAPPING HYDROCARBON SEEPAGE-INDUCED ANOMALIES IN THE ARID REGION, WEST CHINA USING MULTISPECTRAL REMOTE SENSING

Pilong Shi^a, Bihong Fu^{a,*}, Yoshiki Ninomiya^b

^a Institute of Geology and Geophysics, Chinese Academy of Sciences, P.O. Box 9825, Beijing 100029, China - (spl, fubihong)@mail.iggcas.ac.cn

^b Geological Survey of Japan, National Institute of Advanced Industrial Science and Technology, Higashi 1-1-1, Tsukuba 305-8567, Japan - yoshiki.ninomiya@aist.go.jp

KEY WORDS: Hydrocarbon seepages, Rock alterations, Multispectral remote sensing, Kuqa depression, Tian Shan Mountain

ABSTRACT:

Oil and gas reservoir has long-term suffering from hydrocarbon seepages including macroseepages and microseepages. The presence of seepages documents the first element of a hydrocarbon system and could therefore reduce exploration risks. Hydrocarbons that escape from underground reservoirs cause oxidation-reduction reactions either in situ or along vertical migration pathways and result in anomalies in the surface sediments and soils. The surface changes can be detected by multispectral remote sensing. The spectroscopy and ASTER multispectral remote sensing were employed to investigate hydrocarbon seepage-induced anomalies in the Kuqa depression basin, southern Tian Shan Mountain, west China, combined with field investigations, geochemical and mineral analyses of selected samples. Results showed that ASTER band ratios of 2/1 and 4/9 can reveal successfully mineralogical alterations induced by hydrocarbon seepages such as bleached red bed and secondary carbonates in the southern Tian Shan Mountain, which represent an open-window to petroleum system and provide indirect evidence for the presence of hydrocarbon system at depth.

1. INTRODUCTION

Alteration anomalies induced by the hydrocarbon seepages have received considerable attention because of their potential

economic implications for petroleum exploration (Donovan, 1974; Abrams et al., 1984; Petrovic et al., 2008). Hydrocarbons that escape from underground reservoirs cause oxidation-reduction reactions either in situ or along vertical

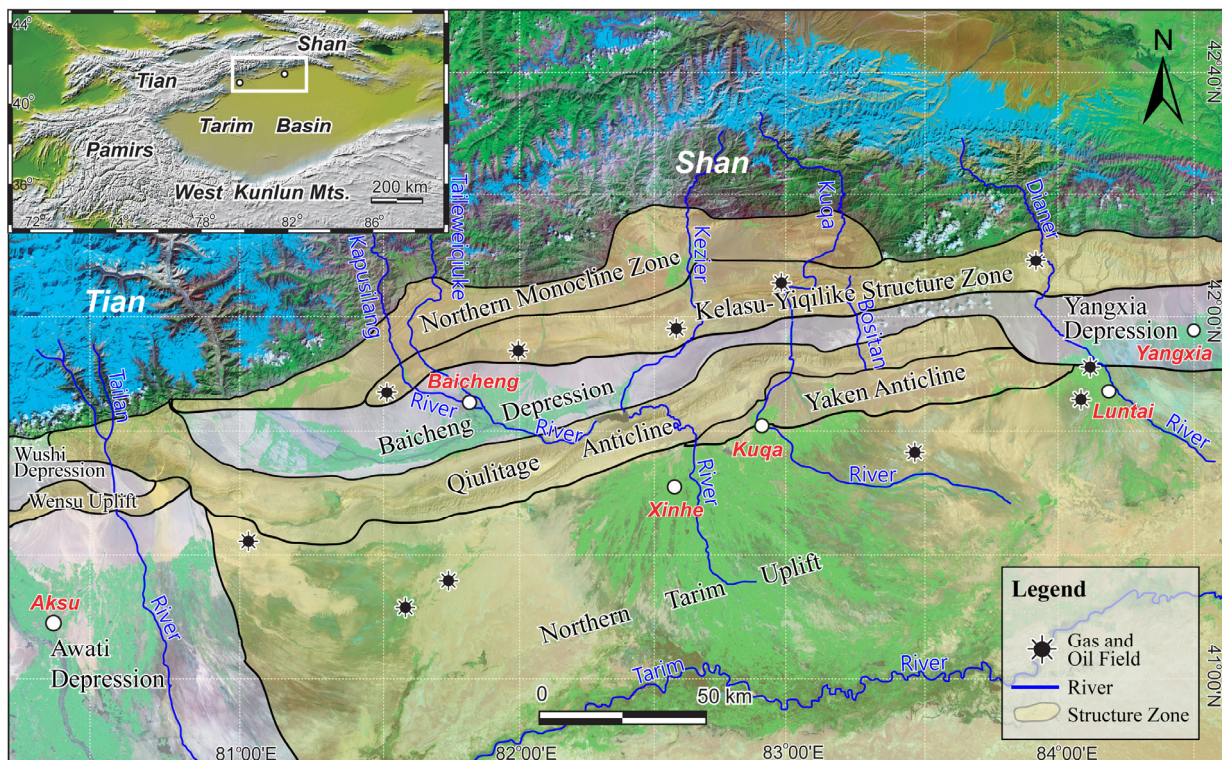


Fig.1 Structure sketch of Kuqa depression basin overlaying on ETM mosaic image.

* Corresponding author.

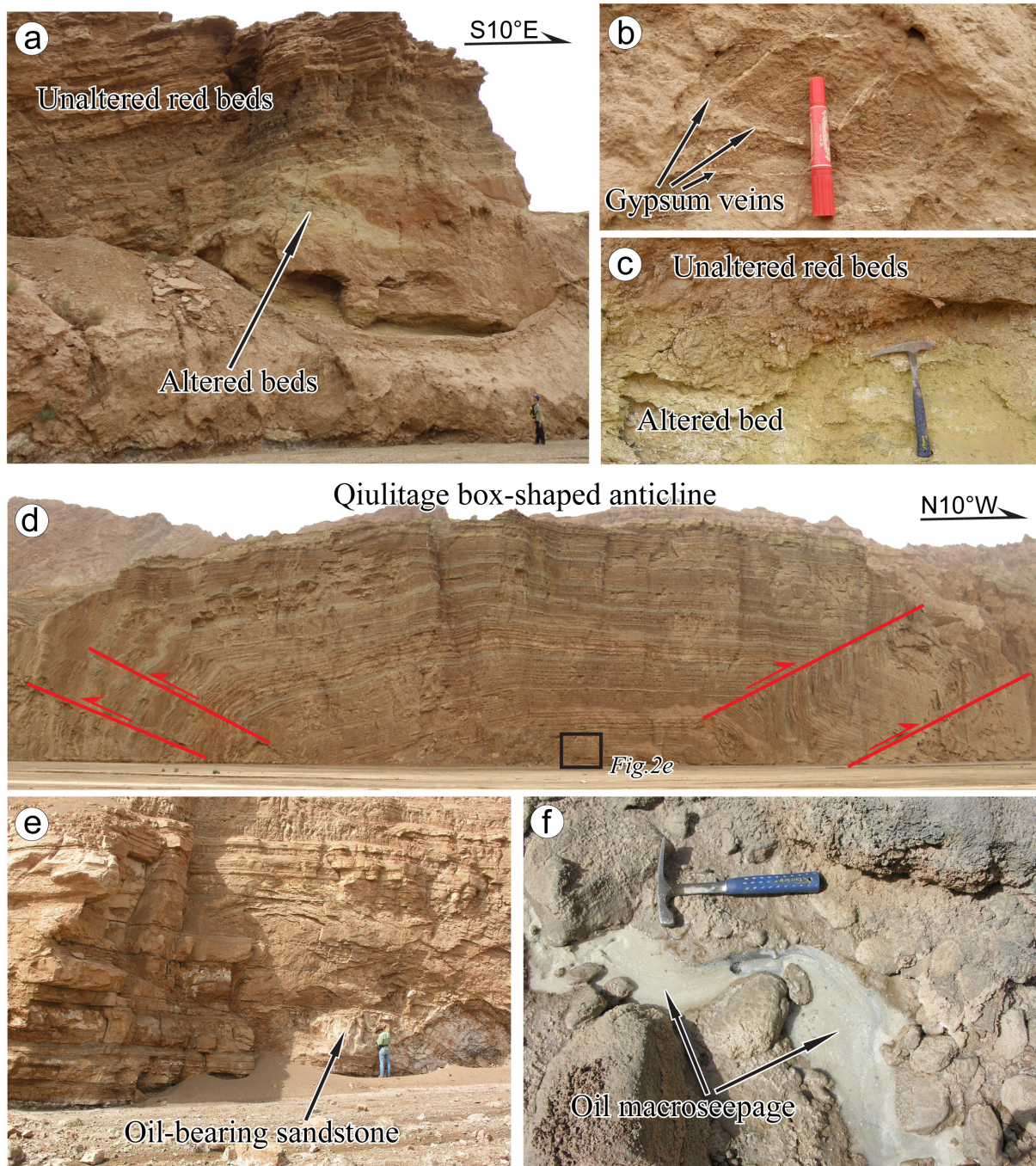


Fig. 2 Photographs showing surface alteration and oil seepage along the Qiulitage anticline. (a). Surface of the altered rocks. Note the alteration of red beds: altered rocks appear as greyish green, yellowish green along the crest of the anticline. (b) Multiple sets of gypsum veins. (c) Surface of the altered rocks in a large scale. (d) Qiulitage box-shaped anticline. (e). Oil-bearing sandstone in the core part of the Qiulitage box-shaped anticline. (f) Oil macroseepage along the Qiulitage anticline.

migration paths and result in anomalies in sediments and soils. Microbial and botanical anomalies; mineralogical alterations; and change of electrical and magnetic properties occur in near-surface sediments (Donovan et al., 1979; Segal and Merin, 1989; Schumacher, 1996). Among these anomalies, bleaching of red beds, enrichment of ferrous iron, alterations of clay minerals and carbonates, and botanical anomalies exhibit diagnostic spectral features that allow detection by remote sensing techniques (Sabins, 1999; Almeida et al., 2002; Fu et al., 2007).

Tonal anomalies and subtle changes in spectral content are used

as important indications in remote sensing for hydrocarbon (Petrovic et al., 2008). Saunders et al. (Saunders et al., 1999) indicated that it can greatly increase the probability of wildcat success and is cost effective in exploration, although the interpretation of remote sensing images along with other field data cannot reveal the depth, size, or quality of reservoirs, or confirm the presence of hydrocarbons. Spectral enhancement, by means of principal component analysis (PCA) and band ratioing of Landsat-7 enhanced thematic mapper plus (ETM+) data, has been successfully used in several studies to recognize surface anomalies and alternation. Almeida et al. (Almeida et

al., 2002) detected the clay mineral and ferric iron distribution in the Serra do Tona Plateau through the application of PCA on six bands of Landsat ETM+. Band ratios of TM have been used to identify the location of ferrous iron (Almeida et al., 1999; Almeida et al., 2002) and bleaching of red beds, clay mineralization, and ferric iron (Freek et al., 2002). However, ASTER VNIR and SWIR data is much powerful for detecting mineralogical alterations induced by hydrocarbon seepages because ASTER sensor has 6 bands comparing with 2 bands of Landsat TM and ETM+ in SWIR region (Ninomiya, 2004; Rowan et al., 2006; Fu et al., 2007; Khan and Mahmood, 2008; Shi et al., 2010).

To investigate hydrocarbon seepage-induced anomalies in the Kuqa depression basin, southern Tian Shan Mountain, west China, spectroscopy and ASTER multispectral remote sensing were used. Geochemical and mineralogical analyses of selected samples using Scanning Electron Microscope with Energy Dispersive Spectrometer (SEM/EDS), thin section study and X-ray diffraction (XRD) were also conducted to determine the relationship between mineral composition, spectral features and surface changes.

2. GEOLOGICAL SETTING

Kuqa depression basin is a Cenozoic rejuvenated foreland basin overlaying above the Permian to the Triassic foreland basin, located on the southern margin of the Tian Shan Mountain (index map in Fig.1) under the typical inland arid to semi-arid climate with sparse vegetation. Previous study and exploration shows that the Kuqa foreland basin has good conditions for hydrocarbon generation and accumulation, and it is a potentially huge oil and gas zones (Huang et al., 1947; Jia et al., 2002).

This area has undergone strongly the Cenozoic tectonic deformation (Burchfiel et al., 1999; Deng et al., 2000; Fu et al., 2003; Sun et al., 2009) and formed several NEE fold-thrust fault structure zone (Fig.1) under strong tectonic compression by Southern Tian Shan orogen. The structure pattern could determine the distribution of oil and gas fields. Many large oil and gas fields were found in the area except Qiulitage Anticline because of complicated structure and geological condition to traditional geophysical exploration technique.

Strata of the East Qiulitage anticline, the study area, could be divided into Jidike formation (N1j) in the core of the anticline, and Kangcun formation (N1k), Kuche formation (N2k) and the Xiyu formation (Q1x) in the flanks. The sedimentary sequence is more than 4000m in thickness. The rocks in the core of the anticline are characterized by red beds interbedded with greyish-green sandstone (Fig.2d). Surface altered rocks appear greyish-green to yellowish green around the core of the anticline (Fig.2a, b, c). Multiple sets of gypsum veins indicate strong tectonic activity. Oil-bearing sandstones and oil macroseepages were found to occur in the crest of the anticline (Fig.2e, f).

3. SPECTRAL MEASUREMENTS AND IMAGE PROCESSING

Spectral reflectance of selected altered and unaltered samples were measured at laboratory using an analytical spectral device (ASD) and the laboratory spectra have been resample to ASTER spectral resolution. Fig.3 illustrates the spectral curves of samples.

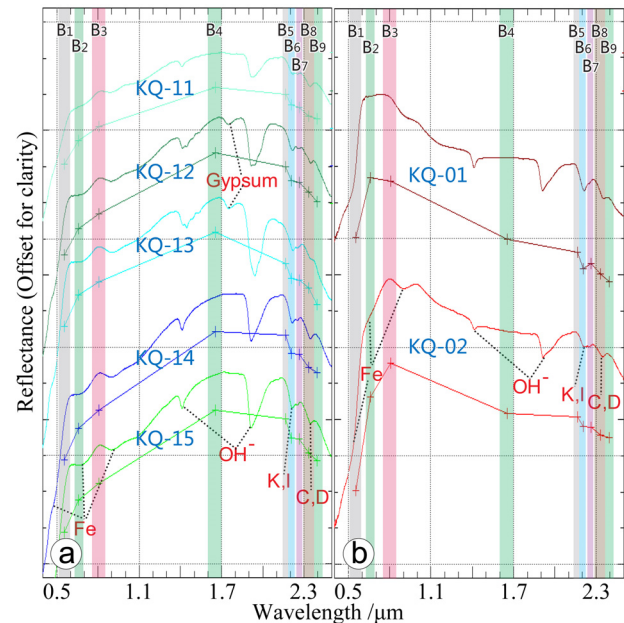


Fig. 3 (a) Reflectance curves of typical altered samples (KQ-11~15) collected from the Qiulitage anticline. Curves with plus symbols are spectra in ASTER spectral resolution resampled from laboratory spectra. Location of the samples is shown in Fig. 4c, d. Diagnostic clay, hydroxyl ion, gypsum and iron absorption features of altered samples are identified by their patterns within the green rectangles. (b) Reflectance curves of unaltered samples (KQ-01, 02) collected from the Qiulitage anticline. I: Illite, K: Kaolinite, C: Calcite, D: Dolomite.

Spectral reflectance features mainly comes from the diagnostic absorption spectrum of ferric ion, hydroxyl ion, gypsum and clay minerals. Unaltered red beds rock samples (Fig.3b) show intense absorption characteristic at $0.56\mu\text{m}$, with relative high reflectance near $0.7\mu\text{m}$, while altered rocks (Fig.3a) appear absorption characteristic at $0.7\mu\text{m}$, thus it's reasonable to extract the distribution information of unaltered red beds containing ferric oxide by the ratio of band 2 to band 1 (b_2/b_1).

Greyish green and yellowish green altered rocks containing ferrous ion minerals show steadily increasing reflectance spectrum between wavelength $1\sim 2\mu\text{m}$, as a result, the content of ferrous oxide could be estimated by the ASTER band ratio b_5/b_4 . Some altered rocks (KQ-12, 13) display characteristic absorption spectrum of gypsum. Compared to unaltered red beds (Fig.3b), greyish green altered rocks (Fig.3a) present more intense absorption characteristic near $1.4\mu\text{m}$, $1.95\mu\text{m}$, $2.21\mu\text{m}$ (band6), and $2.35\mu\text{m}$ (band8, band9), among which, characteristic absorption spectrum near $1.4\mu\text{m}$, $1.95\mu\text{m}$ and $2.21\mu\text{m}$ was engendered by the hydroxyl ion of clay minerals, while the one at $2.35\mu\text{m}$ (band8, band9) was caused by carbonate ion. Meanwhile, altered rocks have relatively high value at ASTER band4, thus, information of carbonate minerals could be extracted by band ratio of b_4/b_9 .

Based on the analysis of the spectral characteristic of selected rock samples above, ASTER data covering the Bositan River and Kuqa River which are in the east of Qiulitage anticline were processed. Greyscale images of ASTER band ratio 2/1 and 4/9 were created (Fig.4a, b). Furthermore, to reveal more abundant information of rocks, false colour image of ASTER band ratio 2/1(R), 3(G) and 4/9(B) was also composited.

Fig.4a, the greyscale image of band ratio of b_2/b_1 , presents the unaltered red beds in white area, because of the high value of

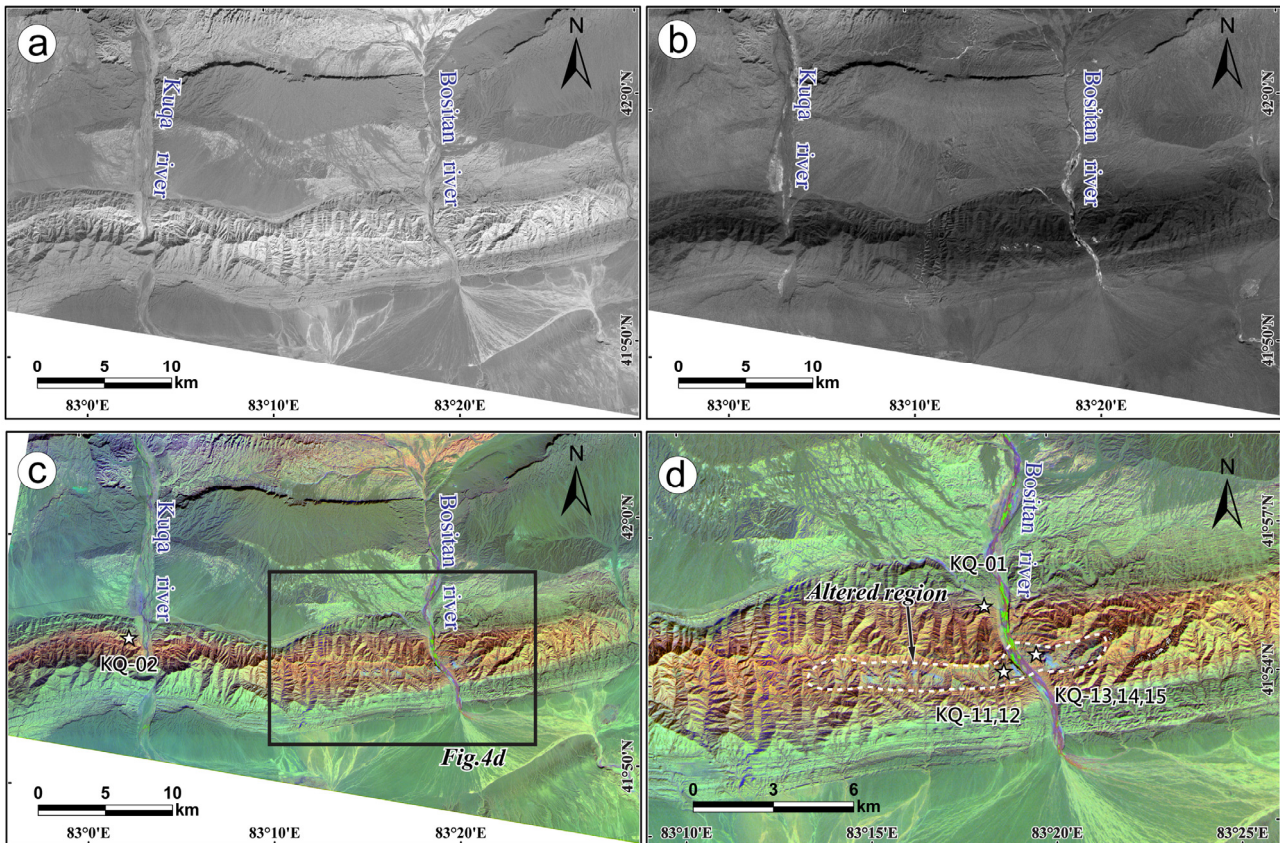


Fig. 4 ASTER images of the study area. (a) Greyscale image of ASTER band ratio 2/1. (b) Greyscale image of ASTER band ratio 4/9. (c) False colour composite image of ASTER band ratio 2/1 (R), 3 (G) and 4/9 (B). (d) Enlarged ASTER false colour composite image. Note altered rocks due to mineralogical alteration induced by hydrocarbon seepage showing as grey-blue to light blue.

band ratio b_2/b_1 resulted from the abundance of ferric oxide minerals. While the altered rocks are displayed as remarkable white area in the greyscale image of band ratio of b_4/b_9 (Fig. 4b) and are significantly different from surrounding area; but it need to be aware that the vegetation along the river valleys appears as white tone too, the confusion need to be analyzed with prior knowledge consequently. According to the band settings and RGB colour composite theory, unaltered rocks appear as yellow, brown tone, while altered rocks appear as gray-blue, light blue in the false colour composite image (Fig. 4c, d). Enlarged ASTER false colour composite image (Fig. 4d) shows altered rocks region and unaltered rocks region can be clearly distinguished. Altered rock region distributes along the crest of Qiulitage anticline and appears as stripe pattern.

4. DISCUSSION

To confirm the relationship between mineral composition, spectral features and surface changes, thin section analyses were performed on altered rocks and they showed the absence of hematite, but more abundance of crystallized, micritic carbonate (Fig. 5a) and calcite cement, while the hematite was the original cement in the unaltered, red unaltered sandstone. Feldspars were surrounded with clay at their margin and along the cleavage planes, indicating the alteration from feldspar to clay mineral. Altered rocks thin section sample also showed the

presence of carbon pitch which indicates ancient petroleum migration. Scanning electron microscopy (SEM) analyses showed the presence of granular calcite mineral particles overlying well developed tabular clay mineral such as kaolinite and illite (Fig. 5b, c) of altered rock sample. X-ray diffraction (XRD) analyses were also carried out to determine mineralogical components of the rock samples collected from the Qiulitage anticline, and the result showed increasing abundance of carbonate mineral such as calcite, dolomite and siderite of hydrocarbon seepage induced altered rock samples (Fig. 6). Therefore, combining analyses with reflectance spectroscopy, thin section study, SEM/EDX and XRD inferred that the carbonate minerals and ferrous oxide minerals in the altered samples are directly related with hydrocarbon seepage. The location of alteration, as well as its intensity, is closely related to the fault system along the Qiulitage anticline. Fault and fracture zone are the main pathways for leaking hydrocarbons. The banding region of hydrocarbon seepage induced altered rock indicated by Fig. 4 distributes at the crest along the Qiulitage anticline; oil macroseepage and rock alteration were found to develop at the crest of Qiulitage anticline in the field near the Kuqa River in the western of Bositan River. Inferred from the discontinuous linear distribution of the region of hydrocarbon seepage induced altered rock, the major pathway of hydrocarbon seepage is the complex fault system along the crest of Qiulitage anticline.

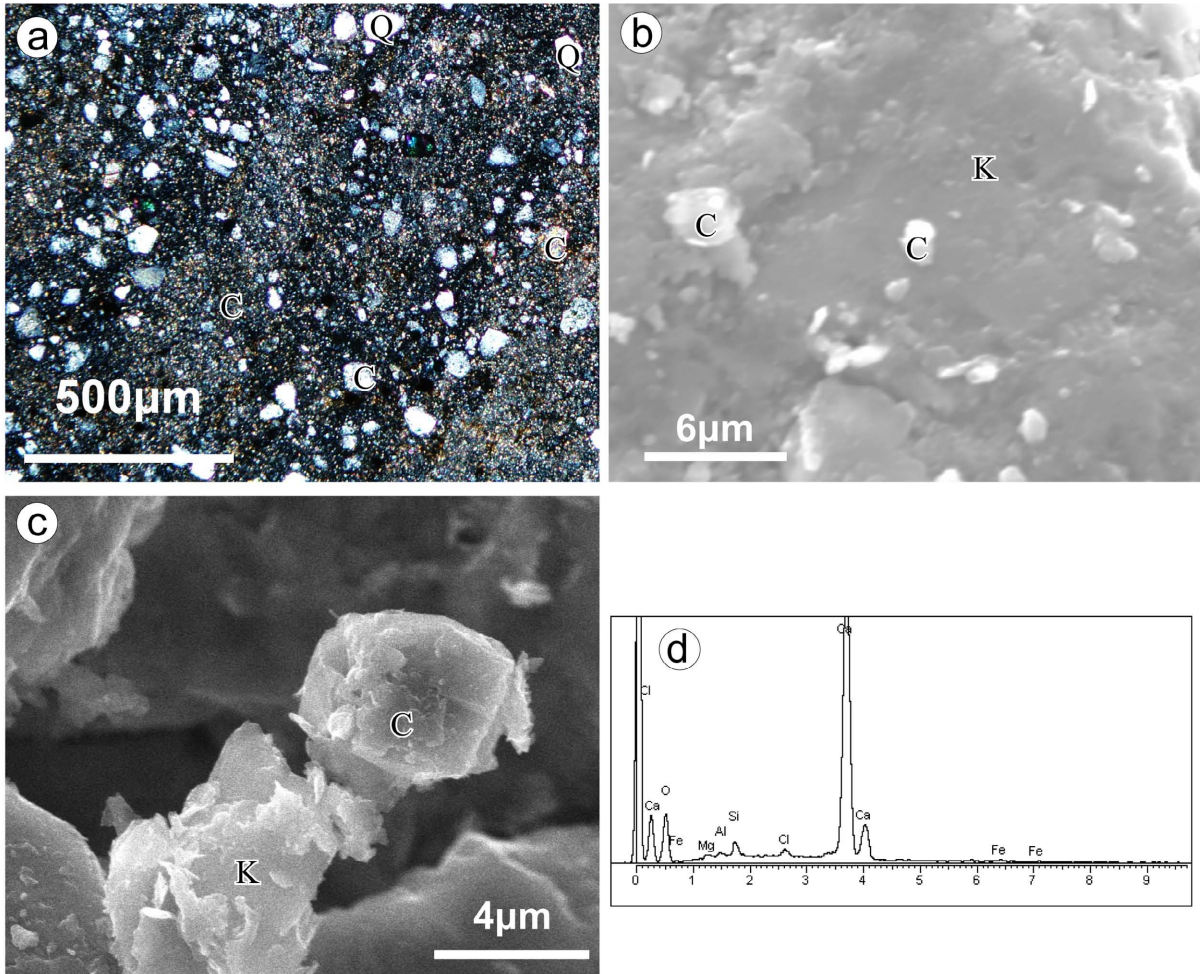


Fig.5 (a) Thin section photo of altered rock sample by orthogonal polarization microscopic study. (2) Scanning electron microscopy (SEM) photo of altered rock sample. Granular calcite mineral particles overlying tabular/platy kaolinite mineral. (3) SEM photo of tabular/platy kaolinite mineral and Granular calcite mineral particles. (4) X-ray energy dispersive spectrum (EDS) of calcite in the altered rock sample. C-Calcite, Q-Quartz, K-kaolinite.

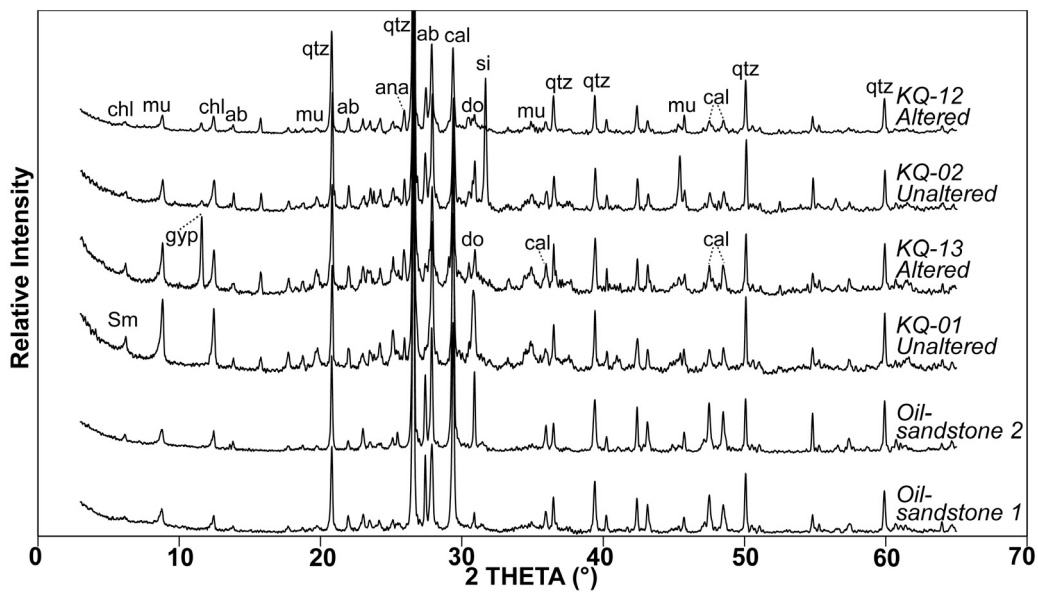


Fig. 6 X-ray diffraction analysis showing mineralogical components of the rock samples collected from the Quiulitage anticline. ab-albite; ana-analcime; cal-calcite; chl-chlorite; do-dolomite; gyp-gypsum; il-illite; mu-muscovite; qtz-quartz; si-siderite; sm-smectite.

5. CONCLUSIONS

Hydrocarbons leaking from subsurface reservoirs can create various surface changes. In this study, we present the mapping of hydrocarbon seepage-induced anomalies in Southern Tian Shan, West China. ASTER band ratio of 2/1 and 4/9 are sensitive to detect iron oxide bearing rocks and carbonate minerals respectively, which can be used to detect the unaltered rocks and altered rocks. The results show that ASTER multispectral images can reveal successfully mineralogical alterations induced by hydrocarbon seepages such as bleached red bed and secondary carbonates, which represent an open-window to petroleum system and provide indirect evidence for the presence of hydrocarbon system at depth. Therefore, the presence of seepages documents the first element of a hydrocarbon system and reduces exploration risks. Field investigations combined with the chemical, spectral and mineralogical analyses in laboratory also demonstrated that these abnormal alterations, revealed by ASTER multi-spectral data, are indeed associated with hydrocarbon seepages.

With better understanding of hydrocarbon microseepage and its surface manifestation, high spatial and spectral resolution spaceborne imaging system like ASTER multispectral imaging system holds great promise as a tool with which to recognize marginal and low relief, structural prospects and stratigraphic traps that are not detected by reflection seismic explorations.

6. ACKNOWLEDGEMENT

This research was funded by the Chinese Major Fundamental Research Developing Project (2006CB202305). The authors are grateful to Prof. Jimin Sun of IGGCAS and Mr. Zhiwu Zhang of China Metallurgical Geology Bureau for their help during the field investigation. Pulong Shi would like to thanks Dr. Aiguo Wang of IGG, CAS for his help in thin section study of samples.

REFERENCES

- Abrams, M.J., Conel, J.E. and Lang, H.R., 1984. *The Joint NASA/Geosat Test case project. Final report, Part 2, Vol. II*. Spec. Publ. Am. Assoc. Petrol. Geol., Tulsa.
- Almeida, R., Miranda, F.P. and Yamakawa, T., 1999. Remote detection of a tonal anomaly in an area of hydrocarbon microseepage, Tucano basin, north-eastern Brazil. *International Journal of Remote Sensing*, 20(13), pp. 2683-2688.
- Almeida, R. et al., 2002. Data integration for a geologic model of hydrocarbon microseepage areas in the Tona Plateau region, North Tucano basin, Brazil. *Canadian Journal Of Remote Sensing*, 28(1), pp. 96-107.
- Burchfiel, B.C. et al., 1999. Crustal shortening on the margins of the Tien Shan, Xinjiang, China. *International Geology Review*, 41(8), pp. 665-700.
- Deng, Q.D. et al., 2000. *Active Tectonics of the Chinese Tianshan Mountains*. Seismological Press, Beijing.
- Donovan, T., Forgey, R. and Roberts, A., 1979. Aeromagnetic detection of diagenetic magnetite over oil fields. *Am. Assoc. Petrol. Geol. Bull.*, 63, pp. 245-248.
- Donovan, T.J., 1974. Petroleum Microseepage at Cement, Oklahoma - Evidence and Mechanism. *Aapg Bulletin-American Association of Petroleum Geologists*, 58(3), pp. 429-446.
- Freek, v.d.M., Dijk, P.v., Werff, H.v.d. and Yang, H., 2002. Remote sensing and petroleum seepage: a review and case study. *Terra Nova*, 14(1), pp. 1-17.
- Fu, B.H., Lin, A.M., Kano, K., Maruyama, T. and Guo, J.M., 2003. Quaternary folding of the eastern Tian Shan, northwest China. *Tectonophysics*, 369(1-2), pp. 79-101.
- Fu, B.H., Zheng, G.D., Ninomiya, Y., Wang, C.Y. and Sun, G.Q., 2007. Mapping hydrocarbon-induced mineralogical alteration in the northern Tian Shan using ASTER multispectral data. *Terra Nova*, 19(4), pp. 225-231.
- Huang, J.Q., Yang, Z.J. and Cheng, Y.Q., 1947. Oilfield geological survey report of Xinjiang *Central Geological Survey Special Report A-No. 21*, pp. 31-66.
- Jia, C.Z., Gu, J.Y. and Zhang, G.Y., 2002. Geological conditions of medium to large gas fields in Kuqa depression. *Chinese Science Bulletin(S1)*, pp. 49-55.
- Khan, S.D. and Mahmood, K., 2008. The application of remote sensing techniques to the study of ophiolites. *Earth-science Reviews*, 89(3-4), pp. 135-143.
- Ninomiya, Y., 2004. Lithologic mapping with multispectral ASTER TIR and SWIR data. *proceedings of SPIE*, 5234, pp. 180-190.
- Petrovic, A., Khan, S.D. and Chafetz, H.S., 2008. Remote detection and geochemical studies for finding hydrocarbon-induced alterations in Lisbon Valley, Utah. *Marine And Petroleum Geology*, 25(8), pp. 696-705.
- Rowan, L.C., Schmidt, R.G. and Mars, J.C., 2006. Distribution of hydrothermally altered rocks in the Reko Diq, Pakistan mineralized area based on spectral analysis of ASTER data. *Remote Sensing of Environment*, 104(1), pp. 74-87.
- Sabins, F.F., 1999. Remote sensing for mineral exploration. *Ore Geology Reviews*, 14(3-4), pp. 157-183.
- Saunders, D.F., Burson, K.R. and Thompson, C.K., 1999. Model for hydrocarbon microseepage and related near-surface alterations. *Aapg Bulletin*, 83(1), pp. 170-185.
- Schumacher, D., 1996. Hydrocarbon-induced alteration of soils and sediments. *AAPG Memoir*, 66, pp. 71-89.
- Segal, D. and Merin, I., 1989. Successful use of Landsat Thematic Mapper data for mapping hydrocarbon microseepage-induced mineralogic alteration, Lisbon Valley, Utah. *Photogrammetric Engineering And Remote Sensing*, 4, pp. 1137-1145.
- Shi, P.L., Fu, B.H. and Ninomiya, Y., 2010. Detecting lithologic features from ASTER VNIR-SWIR multispectral data in the arid region: A case study in the eastern Kalpin uplift, southwest Tian Shan. *Chinese Journal of Geology*, 45(1), pp. 333-347.
- Sun, J.M., Li, Y., Zhang, Z.Q. and Fu, B.H., 2009. Magnetostratigraphic data on Neogene growth folding in the foreland basin of the southern Tianshan Mountains. *Geology*, 37(11), pp. 1051-1054.